CRITICALLY DAMPED STATE AND PHASE DIAGRAM OF ELECTRON DRIFT VELOCITY IN p-i-n SEMICONDUCTORS

NGUYEN PHUOC THE[1,2], LE THI THU THUY[1,2], DINH NHU THAO[3], HO KHAC HIEU[4,a]

[1]Faculty of Environmental and Natural Sciences, Duy Tan University, 03 Quang Trung, Hai Chau, Da Nang 550000, Viet Nam

[2]Institute of Research and Development, Duy Tan University, 03 Quang Trung, Hai Chau, Da Nang 550000, Viet Nam

[3]Faculty of Physics, Hue University of Education, Hue University, 34 Le Loi, Hue, Viet Nam

[4]Faculty of Physics and Chemistry, The University of Da Nang - University of Science and Education, 459 Ton Duc Thang, Hoa Khanh, Da Nang 550000, Viet Nam

Corresponding author[a]: hkhieu@ued.udn.vn

Received December 4, 2025

Abstract. This paper presents a comprehensive investigation of the damped behavior of electron drift velocity in GaAs semiconductors with a p-i-n structure using the ensemble Monte Carlo (EMC) method under the influence of an external electric field. The simulation results show that, in the absence of an external electric field, the electron velocity in the device exhibits a damped oscillatory form if and only if the thickness of the intrinsic semiconductor layer is smaller than a threshold value. Additionally, when the thickness of the intrinsic semiconductor layer is below this critical threshold, an increase in the electric field changes the behavior of electron velocity from under-damped to critically damped and then to over-damped states. In particular, for the first time, we have plotted the phase diagram of electron velocity in phase space of the critical external electric field (E_c) and the thickness (S) of intrinsic semiconductor layer.

Key words: Damped oscillation, EMC simulations, p-i-n structure, Phase diagram of velocity.

DOI: https://doi.org/10.59277/RomJPhys.2026.71.610

1. INTRODUCTION

The transport dynamics of charge carriers in semiconductors play a crucial role in determining the performance and efficiency of modern electronic and optoelectronic devices [1–4]. Understanding these behaviors is essential for optimizing high-speed semiconductor devices, where carrier dynamics at the nanoscale significantly impact device performance [5–7]. In particular, the electron drift velocity in GaAs semiconductors with a p-i-n structure exhibits complex behaviors under the influence of an external electric field [8]. It is worth noting that the drift velocity in this paper refers to the average velocity that charge carriers (electrons or holes) attain in the device under the influence of both internal and external electric fields. The ballistic transport phenomenon, through Raman spectroscopy analysis on GaAs p-i-n semiconductors with a thickness of several hundred nanometers and at a temperature of 300 K, has shown that the electron velocity can reach high values in a short time, such as 150 fs [9]. Furthermore, numerous studies of electronic dynamics in nanoscale devices have revealed intriguing phenomena, including velocity overshoot [9–12], negative differential resistance [13–15], and damped velocity oscillations [16–18]. In particular, we focus on the damped oscillatory behavior of carrier velocity [8, 19]. This phenomenon permits a theoretical framework grounded in carrier kinetics rather than conventional ballistic kinematics. The Monte Carlo method, introduced by Metropolis *et al.* [20], has become a powerful tool for simulating complex physical systems, including semiconductor devices. This computational technique employs statistical sampling to model electron transport phenomena, making it particularly suitable for investigating nanoscale semiconductor structures where classical approaches may fall short [21].

In this study, by applying the ensemble Monte Carlo (EMC) [22, 23] method to a sample of GaAs semiconductor with p-i-n structure, we point out the existence of three common damped behaviors of the electron drift velocity which are so-called the velocity damping states in these devices: (1) the under-damped state, where the system makes several oscillations before reaching equilibrium; (2) the critically damped state, where the oscillating system reaches equilibrium in the shortest time; and (3) the over-damped state, where the damping coefficient is so large that the system does not oscillate and takes a long time to return to equilibrium. Detecting and controlling these velocity damping states is crucial because they significantly affect device performance as well as help identify and control sources of Terahertz oscillations, which originate from plasmons [24, 25]. We simulate and observe these states in GaAs diode samples with p-i-n structure, where the external electric field is the primary impact parameter. By systematically analyzing the transition between under-damped, critically damped, and over-damped states, we provide a comprehensive phase diagram in phase space of the electric field and i-layer thickness.

This article is organized as follows. Section 2 presents the theoretical analysis of the existence of the damping state of the drift velocity in the device based on the well-known momentum relaxation equation [26, 27]. Section 3 introduces our results derived from the EMC simulations. We also discuss the velocity behaviors in the aforementioned diodes and the influence of the external electric field on the velocity behaviors at temperatures 77 K and 300 K. Finally, the conclusions are provided in Section 4.

2. THEORETICAL BACKGROUND

In order to investigate the drift velocity of electrons as well as their characteristics in semiconductors, a theoretical model based on the momentum relaxation equation in the presence of an external electric field is usually used as [26, 27].

$$v' + \Gamma_m v = qE/m^*, \tag{1}$$

where Γ_m is the momentum relaxation rate, m^* is the effective mass, and q is the electron charge.

The above equation describes the drift velocity over time, yielding two solutions where $dv/dt = 0$. One corresponds to the maximum velocity, and the other is the velocity at equilibrium. However, Eq. (1) is only applicable to single-valley semiconductors. For multi-valley semiconductors, the equation can be decomposed into simpler equations for each valley and then combined them together [28, 29]. In semiconductors with satellite valleys, the effective mass is defined as follows [28]

$$m^* = \frac{m_1^* n_1 + m_2^* n_2 + m_3^* n_3 + \dots}{n_1 + n_2 + n_3 + \dots}, \tag{2}$$

where $n_1,\ n_2,\ n_3, \dots$ and $m_1^*,\ m_2^*,\ m_3^*, \dots$ represent the number of electrons and the effective masses in the satellite valleys, respectively.

Momentum and energy relaxation theories can explain ballistic transport and velocity overshoot behaviors under strong external electric fields in nano-structured devices. In the absence of an external electric field, the drift velocity of the carriers still exists under the influence of the internal electric field caused by the charges excited by ultrafast laser pulses with sufficient energy [30, 31]. Optical carriers are generated in the sample according to Beer's law [32, 33]. In this context, the electron velocity varies with time, and Eq. (1) is rewritten accordingly [19]

$$v'' + \Gamma_m v' + \omega_p^2 v = 0, \tag{3}$$

in which ω_p is the angular frequency.

The damped oscillation frequency has the formula as

$$\omega = \sqrt{\omega_p^2 - \frac{\Gamma_m^2}{4}} \tag{4}$$

As we know, the momentum relaxation rate Γ_m depends on the electric field [8, 34], sample thickness, and temperature [9, 19, 35]. And the angular frequency ω_p is dependent on the excited carrier concentration n according to the formula $\omega_p = \sqrt{\frac{nq^2}{m^* \epsilon_s}}$, where ϵ_s is the static dielectric constant. Therefore, the changes in ω_p and Γ_m affect the damping behavior of the velocity. Furthermore, it should be noted that the plasma oscillation period is defined as $T_p = 2\pi/\omega_p$. The relationship between relaxation time $\tau = 1/\Gamma_m$ and plasma oscillation period T_p provides insight into the dynamic behavior of the plasma [36]. In particular, the ratio of the relaxation time to the plasma oscillation period gives an indication of how "collisionless" the plasma is, in which $\tau \gg T_p$ signifies a weakly collisional (or collisionless) regime of charged particles allowing sustained oscillations. While $\tau \ll T_p$ denotes a strongly collisional regime of charged particles where oscillations of velocity are rapidly damped [36, 37].

3. MODELING AND COMPUTATIONAL DETAILS

Based on the theoretical analysis, we use the EMC simulation method combined with a three-valley Γ ($m^* = 0.068m_0$), L ($m^* = 0.22m_0$) and X ($m^* = 0.58m_0$) model (m^* is the effective electron mass of the conduction band in GaAs) to investigate the damping states of electron velocity in the p-i-n GaAs diode at temperatures of 77 K and 300 K under the influence of external electric fields, carrier concentration, and i-layer thickness. The three-valley model (Γ, L, X) is applied (in both the presence and absence of an external electric field) with a spatial resolution along the [100] direction of 10 Å and a time resolution of 0.2 fs. The doping profile in our p-i-n GaAs diode structure is homogeneous, with symmetrically doped p- and n-type layers (each 20 nm thick) on both sides, and an intrinsic (i) layer with variable thickness in the middle. The intrinsic electric field arises from the built-in potential due to the p-i-n junction. We assume the irradiation of ultrashort light pulses with a duration of 12 fs and a central photon energy of 1.49 eV. In our simulation program, the maximum number of simulated carriers is 400,000 superparticles, with each superparticle representing a carrier density on the order of 10^{18} cm^{-3}. The actual number of simulated superparticles depends on the excitation carrier concentration and the physical dimensions of the device. Carriers are injected into and exit the device only through the contacts. At all other surfaces, carriers are reflected at the device boundaries. The scattering processes considered in our simulation include phonon scatterings (acoustic phonon, polar optical phonon, and intervalley optical phonon), plasmon scatterings, impurity scatterings, and electron-electron scatterings.

We did take holes into account in our calculations; however, due to their large effective mass, the hole drift velocity is extremely small-typically orders of magnitude lower than that of electrons. As a result, their contribution to the relevant quantities is negligible and can be reasonably omitted. In this simulation, electron-hole recombination was also not considered, under the assumption that electrons, driven by both the internal and external electric fields, move sufficiently fast such that the probability of recombination with holes remains very low within the timescale of interest.

Coulomb interactions between charge carriers (electrons and holes) are generally classified into two components: short-range and long-range interactions. In the present study, both types of interactions are taken into account. During the simulation, the Poisson equation is solved to obtain the electrostatic potential distribution within the device, which corresponds to the long-range Coulomb interaction. The time step used in the simulation is set to 0.2 fs, which is significantly smaller than the plasma oscillation period, ensuring that the influence of plasma oscillations is accurately captured in the results. There exist various approaches for evaluating short-range interactions. In this work, we employ the following method: the simulation domain is divided into mesh cells of a size comparable to the Debye wavelength. For each particle within a cell, we consider its interactions with particles located in the 27 neighboring cells forming a surrounding cube.

In solving the Poisson equation, both Dirichlet and Neumann boundary conditions – pertaining to the values of the potential and its derivatives – are incorporated into the simulation. The values of the potential and its derivatives at the boundaries are assigned appropriately, depending on the specific location at which the potential is evaluated. Due to the technical nature of these details, we refrain from presenting them here.

4. RESULTS AND DISCUSSION

In Fig. 1, we show the drift velocity of electrons in the p-i-n GaAs diode as a function of time at temperatures 77 K and 300 K without an external electric field. The carrier concentration was set to 10^{18} cm^{-3}. The investigation was carried out with various thicknesses (200 nm, 500 nm, and 1200 nm at temperature 77 K (Fig. 1a); and 200 nm, 400 nm, and 800 nm at temperature 300 K (Fig. 1b)) of intrinsic (i) semiconductor layer. As can be observed from Fig. 1, the plots clearly indicate the under-damped state of the electron drift velocity, especially for the thicknesses of 200 nm and 500 nm at 77 K (Fig. 1a), and 200 nm and 400 nm at 300 K (Fig. 1b). And the damped oscillations gradually decrease in amplitude during the velocity relaxation process as the device thickness increases. The maximum drift velocity are 4.3×10^7 cm/s, 3.1×10^7 cm/s, and 2.2×10^7 cm/s for the thicknesses of 200 nm, 400 nm, and 800 nm, respectively.

As realized from the simulation results, in the under-damped state, the number of oscillations before returning to equilibrium depends on the i-layer thickness; the smaller the thickness, the greater the number of oscillations. When the thickness exceeds a certain value (referred to as a critical thickness), the velocity begins to transit to an over-damped state, and this phenomenon is consistent with observations in many previous studies. Furthermore, we found out that in the absence of the external electric field, the damped oscillation behavior only exists when the thickness of intrinsic semiconductor layer is smaller than the critical thickness. In our simulations, we obtain the critical thickness about 1 µm for the p-i-n GaAs diode at temperature 300 K, as shown in Fig. 2. If the thickness of i-layer exceeds the critical threshold, the damped oscillation behavior of the electron velocity does not occur; instead, we observe only the overshoot behavior of the velocity. This is why, in many previous

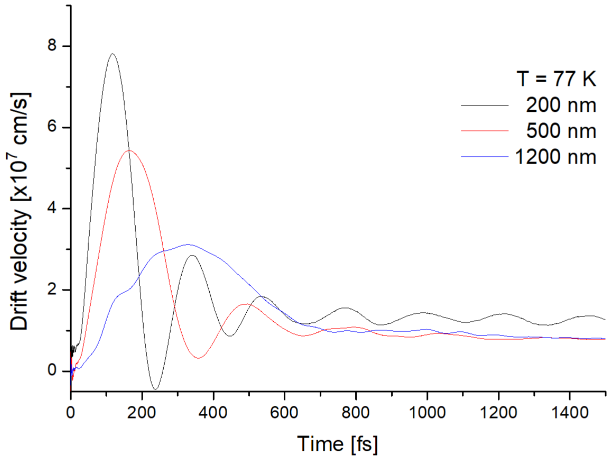

(a)

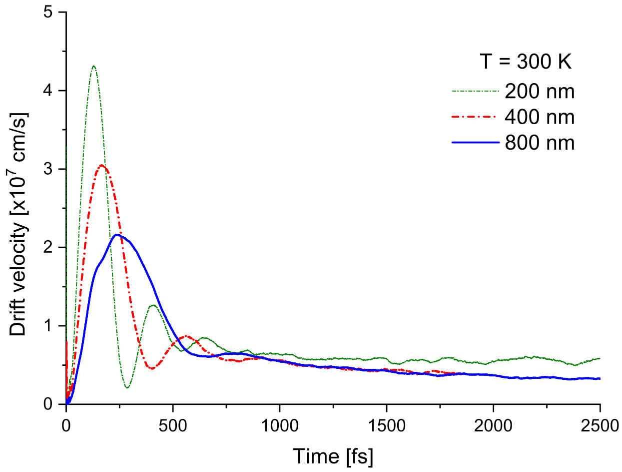

(b)

Fig. 1 – Velocity over time with various sample thicknesses of p-i-n GaAs diode at a) 77 K [8] and b) 300 K.

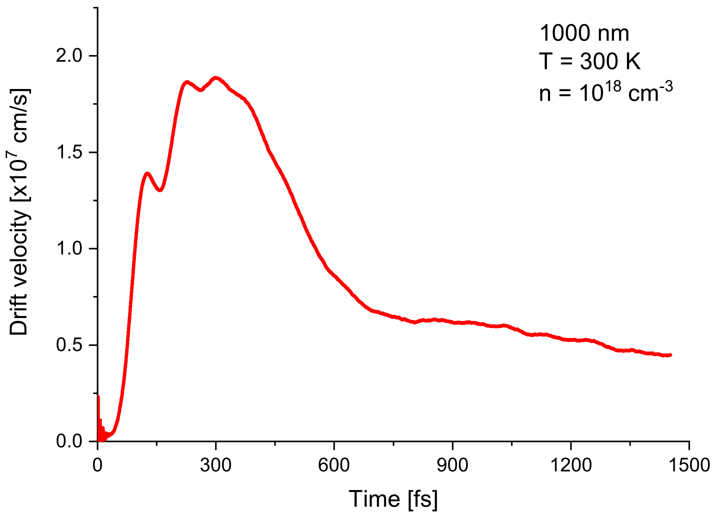

Fig. 2 – Velocity over time with 1000 nm thickness of i-layer of p-i-n GaAs diode.

studies focusing exclusively on devices with large thicknesses under high external electric fields, only the over-damped state associated with velocity overshoot behavior was observed.

The existence of critical thickness can be elucidated as follows: As discussed in relation to Eq. (4), the damped oscillation frequency depends on the thickness of the sample. Consequently, variations in thickness lead to corresponding changes in the damped oscillation frequency due to the interplay between collisions of charged particles and plasma oscillations. If $\tau \gg T_p$ the under-damped velocity state is observed; whereas in the opposite case, the velocity exhibits over-damped behavior. Additionally, the results also indicate that the standard ballistic mechanism of electrons not only exists at 150 fs and then returns to equilibrium as indicated in previous articles, but also varies with thickness and repeats several times after each period before reaching equilibrium state.

After determining the critical thickness, we investigate the influence of the external electric field on the damping state. A sample with an intrinsic semiconductor layer (i) of 400 nm in the p-i-n GaAs diode was chosen to study the velocity behaviors. The external electric field was increased in intervals of 20 kV/cm, from 0 to 400 kV/cm. Here it should be noted that in our simulations, the electric fields reach up to 400 kV/cm, approaching or exceeding the onset of impact ionization [38]. However, for the sake of computational simplicity, impact ionization has been neglected

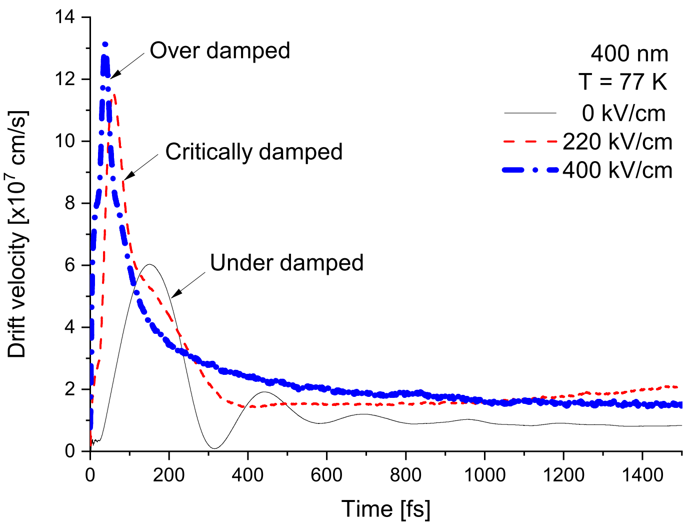

Fig. 3 – Damping states in p-i-n GaAs device sample at 77 K with a 400 nm i-layer of p-i-n GaAs diode.

in our study. In Fig. 3, we show the drift velocity of electrons as a function of time at three different external electric fields. The existence of three damping states of electron drift velocity can be observed in this figure. The electron drift velocity transitions from the under-damped to a critically damped, and eventually to an over-damped state. We have determined that the critical electric field value (E_c) for the p-i-n GaAs diode with an i-layer of 400 nm at a temperature of 77 K is approximately 220 kV/cm. A similar transition occurs at 300 K, but the critical electric field value decreases with the increasing temperature; particularly, under the same i-layer thickness and concentration conditions, the critical value for GaAs is approximately 60 kV/cm. These results clearly show that when temperature and carrier concentration are constant, the damping states of the electron velocity in this device strongly depend on the external electric field. Here it should be noted that in the absence of an external electric field, the existence of damping oscillation states of the velocity is attributed to the spatial distribution of photo-excited electrons and holes. This distribution leads to the formation of an internal electric field, which induces the oscillation of plasmons. Consequently, the oscillation of drift velocity, and thus the oscillation of the electric field, is observed [13, 39], as displayed in Fig. 4.

Nevertheless, an important parameter that also affects the damping states is the concentration of photo-excited electrons, which alters the angular frequency accord-

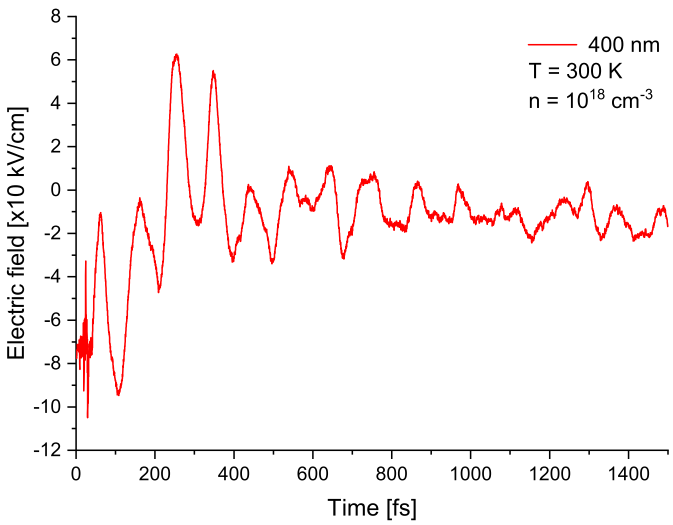

Fig. 4 – The fluctuation of internal electric field *versus* time at temperature 300 K with photo-excited carrier concentration 10^{18} cm^{-3}.

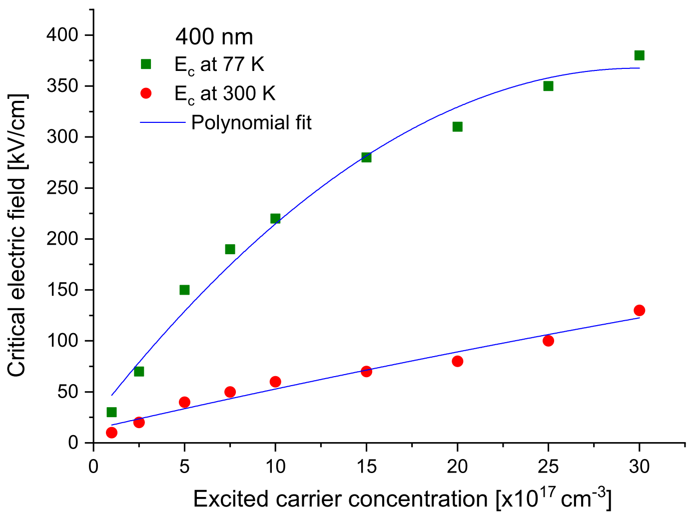

Fig. 5 – The dependence of critical electric field on photo-excited carrier concentration in p-i-n GaAs diode at temperatures 77 K and 300 K.

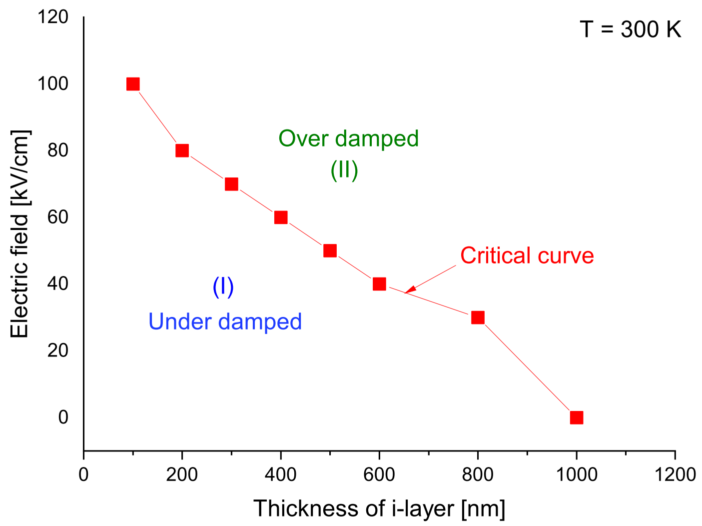

Fig. 6 – Phase diagram in (E_c, S) space in p-i-n GaAs diode at temperature 300 K.

ing to the formula $\omega_p = \sqrt{\frac{nq^2}{m^*\epsilon_s}}$. Therefore, it is necessary to adjust the electric field to bring the velocity to the critical state when the carrier concentration n changes. To address this, we analyze the above sample to determine the critical electric field values for carrier concentrations ranging from 10^{17} to 3×10^{18} cm^{-3}. The results of this investigation are shown in Fig. 5, where the critical electric field is plotted *versus* the carrier concentration of the p-i-n GaAs diode at temperatures of 77 K and 300 K. As can be observed from this figure, temperature changes also affect the critical values of the electric field.

The results obtained from Figs. 1, 3, and 5 reveal that there are several factors contributing to the damping of electron velocity such as i-layer thickness (see Fig. 1), electric field (see Fig. 3), excited carrier concentration and temperature (see Fig. 5). In order to clearly demonstrate the existence of under-damped and over-damped states in relation to i-layer thickness and external field, we investigate and derive the critical values of the electric field at different thicknesses. Figure 6 presents the phase diagram (E_c, S) for the p-i-n GaAs diode at temperature of 300 K. The critical curve separates the phase space into two regions: under-damped state (region (I)) and over-damped state (region (II)) of the electron drift velocity. This indicates that at the specific temperature and carrier concentration conditions, the under-damped state exists when the i-layer thickness and external electric field are below their critical values. If the external electric field is high and the i-layer thickness exceeds the critical value, the velocity transitions to the over-damped state. In other words, as the i-layer thickness decreases, a stronger external electric field is required to shift the velocity from the under-damped to the over-damped state. Our findings reveal that the external electric field serves as a control parameter that dictates the transition between different damping states, with the critical values of the field and i-layer thickness defining the boundary between under-damped and over-damped behavior.

5. CONCLUSION

In this work, we present an investigation of the damped behavior of electron drift velocity in GaAs semiconductors with a p-i-n structure using the EMC method. We observed three damping oscillation states of the electron drift velocity in the p-i-n GaAs diode when changing the external electric field. Under specific temperature, thickness, and carrier concentration conditions, the electric field serves as a control parameter to shift the state from under-damped to critically damped and then to over-damped. We have plotted the phase diagram of electron velocity in phase space of the critical external electric field and i-layer thickness. The diagram clearly shows that the critical curve separates the phase space into two regions: region (I), the under-damped state, and region (II), the over-damped state. Additionally, the results indicate that when there is no external electric field, the standard ballistic mechanism of velocity not only exists in the initial short time but also repeats many times after each period depending on the i-layer thickness. The results of this investigation provide deeper insights into nano semiconductor devices, highlighting effects that have been previously overlooked in the field.

REFERENCES

1. A. Troisi, D. L. Cheung, and D. Andrienko, Phys. Rev. Lett. **102**, 116602 (2009); https://doi.org/10.1103/PhysRevLett.102.116602.
2. C. R. Drago and A. Majorana, Transport Theory and Statistical Physics **29**, 805 (2000); https://doi.org/10.1080/00411450008200003.
3. C. Zhang, L. Cheng, and Y. Liu, Phys. Rev. B **102**, 115405 (2020); https://doi.org/10.1103/PhysRevB.102.115405.
4. S. Giannini and J. Blumberger, Acc. Chem. Res. **55**, 819 (2022); https://doi.org/10.1021/acs.accounts.1c00675.
5. V. Sverdlov, E. Ungersboeck, H. Kosina, and S. Selberherr, Materials Science and Engineering: R: Reports **58**, 228 (2008); https://doi.org/10.1016/j.mser.2007.11.001.
6. M. Aydın, S. Mutlu, A. Erol, J. Puustinen, J. Hilska, M. Guina, and O. Donmez, Physica Status Solidi (RRL) – Rapid Research Letters **16**, 2200204 (2022); https://doi.org/10.1002/pssr.202200204.
7. Y. Yun, S. Wu, D. Wang, X. Luo, J. Chen, G. Wang, A. Takao, and L. Wan, Measurement **241**, 115708 (2025); https://doi.org/10.1016/j.measurement.2024.115708.

8. N. P. The, D. N. Thao, and H. K. Hieu, Physics Letters A **490**, 129174 (2023); https://doi.org/10.1016/j.physleta.2023.129174.
9. S. Wang, Z. Wu, Z. Haifeng, X. Duan, C. Han, Y. Wei, and H. Liu, Solid State Communications **288**, 68 (2019); https://doi.org/10.1016/j.ssc.2018.11.018.
10. E. D. Grann, K. T. Tsen, O. F. Sankey, D. K. Ferry, A. Salvador, A. Botcharev, and H. Morkoç, Applied Physics Letters **67**, 1760 (1995); https://doi.org/10.1063/1.115041.
11. J. M. Iglesias, E. Pascual, S. García-Sánchez, and R. Rengel, Applied Physics Letters **123**, 052105 (2023); https://doi.org/10.1063/5.0152078.
12. Y. Seok, H. Jang, Y. Choi, Y. Ko, M. Kim, H. Im, K. Watanabe, T. Taniguchi, J. H. Seol, S.-S. Chee, *et al.*, ACS Nano **18**, 8099 (2024); https://doi.org/10.1021/acsnano.3c11613.
13. K. W. Boer, *Introduction to Space Charge Effects in Semiconductors* (Springer Berlin, Heidelberg, 2009).
14. O. Donmez, M. Aydın, S. Mutlu, J. Puustinen, J. Hilska, M. Guina, and A. Erol, Materials Science in Semiconductor Processing **154**, 107227 (2023); https://doi.org/10.1016/j.mssp.2022.107227.
15. P. S. Padhi, S. K. Rai, K. Vijay, H. Srivastava, R. S. Ajimsha, S. Banik, A. K. Srivastava, and P. Misra, ACS Appl. Nano Mater. (2024); https://doi.org/10.1021/acsanm.4c02024.
16. G. M. Moatimid, T. S. Amer, and W. S. Amer, Scientific Reports **13**, 6507 (2023); https://doi.org/10.1038/s41598-023-33461-z.
17. Y. Guo, Z. Xu, A. G. Curto, Y.-J. Zeng, and D. Van Thourhout, Progress in Materials Science **138**, 101158 (2023); https://doi.org/10.1016/j.pmatsci.2023.101158.
18. H. M. Abrar, U. Shabbir, S. A. Khan, and M. Khan, Zeitschrift für Naturforschung A **78**, 113 (2023); https://doi.org/10.1515/zna-2022-0180.
19. N. P. The, H. N. Toan, D. N. Thao, and H. K. Hieu, Physics Letters A **445**, 128240 (2022); https://doi.org/10.1016/j.physleta.2022.128240.
20. N. Metropolis, A. W. Rosenbluth, M. N. Rosenbluth, A. H. Teller, and E. Teller, The Journal of Chemical Physics **21**, 1087 (1953); https://doi.org/10.1063/1.1699114.
21. C. Jacoboni and L. Reggiani, Rev. Mod. Phys. **55**, 645 (1983); https://doi.org/10.1103/RevModPhys.55.645.
22. K. Tomizawa, *Numerical Simulation of Submicron Semiconductor Devices* (1st edn., Artech House, Boston, 1993).
23. P. Priyadarshi and N. Neophytou, Journal of Applied Physics **133**, 054301 (2023); https://doi.org/10.1063/5.0134466.
24. A. Singh, H. Němec, J. Kunc, and P. Kužel, Phys. Rev. Res. **6**, 033063 (2024); https://doi.org/10.1103/PhysRevResearch.6.033063.
25. J. M. Caridad, S. Castelló, S. M. López Baptista, T. Taniguchi, K. Watanabe, H. G. Roskos, and J. A. Delgado-Notario, Nano Lett. **24**, 935 (2024); https://doi.org/10.1021/acs.nanolett.3c04300.
26. M. O. Vassell and J. Lee, Journal of Applied Physics **58**, 4230 (1985); https://doi.org/10.1063/1.335557.
27. N. P. The and H. K. Hieu, Physics Letters A **383**, 2314 (2019); https://doi.org/10.1016/j.physleta.2019.04.034.
28. B. E. Foutz, S. K. O'Leary, M. S. Shur, and L. F. Eastman, MRS Proceedings **512**, 555 (1998).
29. K. Blotekjaer, IEEE Transactions on Electron Devices **17**, 38 (1970); https://doi.org/10.1109/T-ED.1970.16921.
30. J. Zhao, R. Nughays, O. M. Bakr, and O. F. Mohammed, J. Phys. Chem. C **125**, 14495 (2021); https://doi.org/10.1021/acs.jpcc.1c02433.
31. X. Lu, D. Huang, G. Gumbs, T. T. Clark, and A. Sharma, Phys. Rev. B **111**, 115302 (2025); https://doi.org/10.1103/PhysRevB.111.115302.

32. Beer, Annalen der Physik **162**, 78 (1852); https://doi.org/10.1002/andp.18521620505.
33. H. G. Pfeiffer and H. A. Liebhafsky, J. Chem. Educ. **28**, 123 (1951); https://doi.org/10.1021/ed028p123.
34. S. Teitel and J. W. Wilkins, Journal of Applied Physics **53**, 5006 (1982); https://doi.org/10.1063/1.331376.
35. G. Baccarani and M. Wordeman, Solid-State Electronics **28**, 407 (1985); https://doi.org/10.1016/0038-1101(85)90100-5.
36. J. A. Bittencourt, *Fundamentals of Plasma Physics* (3rd edn., Springer New York, NY, 2004).
37. J. W. Edenstrasser and M. M. M. Kassab, Journal of Plasma Physics **56**, 45–65 (1996); https://doi.org/10.1017/S0022377800019085.
38. C. Groves, R. Ghin, J. David, and G. Rees, IEEE Transactions on Electron Devices **50**, 2027 (2003).
39. P. N. Butcher, Reports on Progress in Physics **30**, 97 (1967); https://doi.org/10.1088/0034-4885/30/1/303.